Solution ^{1}H NMR of the Molecular and Electronic Structure of the Heme Cavity and Substrate Binding Pocket of High-Spin Ferric Horseradish Peroxidase: Effect of His42Ala Mutation

Anbanandam Asokan,[†] Jeffrey S. de Ropp,[‡] Sherri L.Newmyer,[§] Paul R. Ortiz de Montellano,[§] and Gerd N. La Mar*[,†]

Contribution from the Department of Chemistry and NMR Facility, University of California, One Shields Avenue, Davis, California 95616, and Department of Pharmaceutical Chemistry, University of California, San Francisco, California 94143

Received October 16, 2000. Revised Manuscript Received February 2, 2001

Abstract: Solution ^{1}H NMR has been used to assign a major portion of the heme environment and the substrate-binding pocket of resting state horseradish peroxidase, HRP, despite the high-spin iron(III) paramagnetism, and a quantitative interpretive basis of the hyperfine shifts is established. The effective assignment protocol included 2D NMR over a wide range of temperatures to locate residues shifted by paramagnetism, relaxation analysis, and use of dipolar shifts predicted from the crystal structure by an axial paramagnetic susceptibility tensor normal to the heme. The most effective use of the dipolar shifts, however, is in the form of their temperature gradients, rather than by their direct estimation as the difference of observed and diamagnetic shifts. The extensive assignments allowed the quantitative determination of the axial magnetic anisotropy, $\Delta\chi_{ax} = -2.50 \times 10^{-8}$ m^3/mol, oriented essentially normal to the heme. The value of $\Delta\chi_{ax}$ together with the confirmed T^{-2} dependence allow an estimate of the zero-field splitting constant $D = 15.3$ cm^{-1}, which is consistent with pentacoordination of HRP. The solution structure was generally indistinguishable from that in the crystal (Gajhede, M.; Schuller, D. J.; Henriksen, A.; Smith, A. T.; Poulos, T. L. *Nature Structural Biology* **1997**, *4*, 1032−1038) except for Phe68 of the substrate-binding pocket, which was found turned into the pocket as found in the crystal only upon substrate binding (Henriksen, A.; Schuller, D. J.; Meno, K.; Welinder, K. G.; Smith, A. T.; Gajhede, M. *Biochemistry* **1998**, *37*, 8054−8060). The reorientation of several rings in the aromatic cluster adjacent to the proximal His170 is found to be slow on the NMR time scale, confirming a dense, closely packed, and dynamically stable proximal side up to 55 °C. Similar assignments on the H42A-HRP mutant reveal conserved orientations for the majority of residues, and only a very small decrease in $\Delta\chi_{ax}$ or *D*, which dictates that five-coordination is retained in the mutant. The two residues adjacent to residue 42, Ile53 and Leu138, reorient slightly in the mutant H42A protein. It is concluded that effective and very informative ^{1}H NMR studies of the effect of either substrate binding or mutation can be carried out on resting state heme peroxidases.

Introduction

Horseradish peroxidase, HRP,[1] a 44 kDa single chain heme glycoprotein that oxidizes aromatic substrates at the expense of peroxide, is probably the most studied enzyme and has served as the model for the development of Michaelis−Menten kinetics.[2−7] The key distal catalytic residues in the activation of the enzyme by H_2O_2 are the distal His42, which serves a general base, and Arg38, whose side chain facilitates charge separation in the cleavage of the peroxide bond. Mutating His42 reduces[8] the activation rate by $\sim 10^6$. The aromatic reducing substrate of HRP binds at the heme edge[5] where there are located several aromatic residues whose mutation influences substrate binding.[9−11] In the absence of a crystal structure, early solution NMR studies had provided a qualitative description of the heme pocket by using other crystallographically characterized heme peroxidases as homology models.[11−29] The proposed active site

* Address correspondence to this author. Phone: (530) 752-0958. FAX: (530) 752-8995. E-mail: lamar@indigo.ucdavis.edu.

† Department of Chemistry, University of California, Davis.

‡ NMR Facilit, University of California, Davis.

§ Department of Pharmaceutical Chemistry, University of California, San Francisco.

(1) Abbreviations used: benzhydroxamic acid, BHA; horseradish peroxidase, HRP; cyanide-ligated horseradish peroxidase, HRP-CN; met(ferric) myoglobin, metMb; two-dimensional nuclear Overhauser spectroscopy, NOESY; peanut peroxidase, PNP; total correlation spectroscopy, TOCSY; wild-type, WT; recombinant wild-type, rWT.

(2) Welinder, K. G. In *Plant Peroxidases 1980−1990: Topics and Detailed Literature on Molecular, Biochemical, and Physiological Aspects*; Penel, C., Gaspar, T., Greppin, H., Eds.; University of Geneva: Switzerland, 1992; pp 1−24.

(3) Poulos, T. L. *Curr. Opin. Biotechnol.* **1993**, *4*, 484−489.

(4) Poulos, T. L.; Fenna, R. E. In *Metal Ions in Biological Systems*; Sigel, H., Ed.; Marcel Dekker: New York, 1994; pp 25−75.

(5) Ortiz de Montellano, P. R. *Annu. Rev. Pharmacol. Toxicol.* **1992**, *32*, 89−107.

(6) English, A. M.; Tsaprailis, G. *Adv. Inorg. Chem.* **1995**, *43*, 79−125.

(7) Dunford, H. B. *Peroxidases in Chemistry and Biology*; CRC Press: Boca Raton, FL, 1991; Vol. 2.

(8) Newmyer, S. L.; Ortiz de Montellano, P. R. *J. Biol. Chem.* **1995**, *270*, 19430−19438.

(9) Gilfoyle, D. J.; Rodriguez-Lopez, J. N.; Smith, A. T. *Eur. J. Biochem.* **1996**, *236*, 714−722.

(10) Veitch, N. C.; Gilfoyle, D. J.; White, C. G.; Smith, A. T. In *Plant Peroxidases: Biochemistry and Physiology*; Obinger, C., Burner, U., Ebermann, R., Penel, C., Greppin, H., Eds.; University of Geneva: Switzerland, 1996; pp 1−6.

(11) Veitch, N. C.; Gao, Y.; Smith, A. T.; White, C. G. *Biochemistry* **1997**, *36*, 14751−14761.

10.1021/ja003687w CCC: $20.00
Published on Web 04/13/2001

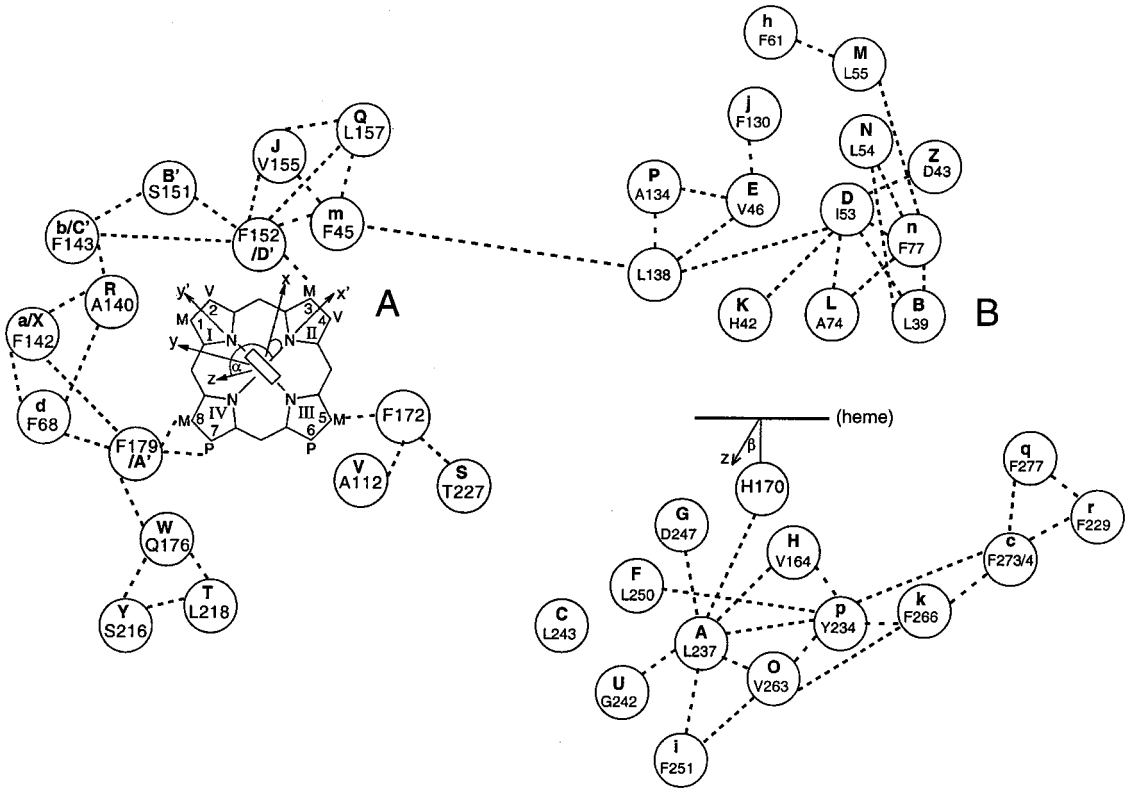

Figure 1. Schematic representation of primarily peripheral (A) and primarily axial (B) residues in the "second sphere" of the heme in the crystal structure of HRP that are assigned herein. Dashed lines indicate observed dipolar contacts. The residues are labeled both in the symbol of the spin system and the residue type and sequence number. The iron-centered reference coordinate system, x', y', z', is shown in which the geometric factors for the dipolar shift are calculated. The major magnetic axis, z, of the expected axially symmetric paramagnetic susceptibility tensor may be tilted from the heme normal by an angle β (B) in a direction defined by the angle α between the projection of the z magnetic axis on the heme plane and the x' axis (A).

structure was largely confirmed by the recent crystal structure of HRP.[30] The paramagnetism of functional forms of HRP imparts large hyperfine shifts, δ_{hf}, composed of contact and dipolar shifts that facilitate spectral resolution, but also degrades the efficiency of NMR experiments.[23,31,32] However, 2D experiments appropriately tailored[31−33] to relaxed resonances are remarkably effective in assigning and locating residues near the heme.

The dipolar component of the hyperfine shift for nonligated residues is of prime interest, and is given by:[32−35]

$$\delta^{i}_{dip} = (24\pi N_A)^{-1}[2\Delta\chi_{ax}(3\cos^2\theta'_i - 1)R_{Fe-i}^{-3} + 3\Delta\chi_{rh}(\sin^2\theta'_j \cos 2\Omega'_i)R_{Fe-i}^{-3}]\Gamma(\alpha,\beta,\gamma) \quad (1)$$

where θ', Ω', and R_{Fe-i} are the polar coordinates of proton i in an arbitrary, iron-centered coordinated system with axes x', y', z'. α, β, γ are the Euler angles that rotate this reference coordinate system into the magnetic coordinate system, x, y, z (Figure 1A), and $\Delta\chi_{ax}$ and $\Delta\chi_{rh}$ are the axial and rhombic

(12) La Mar, G. N.; de Ropp, J. S.; Smith, K. M.; Langry, K. C. *J. Biol. Chem.* **1980**, *255*, 6646−6652.
(13) Sakurada, J.; Takahashi, S.; Hosoya, T. *J. Biol. Chem.* **1986**, *261*, 9657−9662.
(14) Thanabal, V.; de Ropp, J. S.; La Mar, G. N. *J. Am. Chem. Soc.* **1987**, *109*, 7516−7525.
(15) Thanabal, V.; de Ropp, J. S.; La Mar, G. N. *J. Am. Chem. Soc.* **1988**, *110*, 3027−3035.
(16) Thanabal, V.; La Mar, G. N.; de Ropp, J. S. *Biochemistry* **1988**, *27*, 5400−5407.
(17) Veitch, N. C.; Williams, R. J. P. *Eur. J. Biochem.* **1990**, *189*, 351−362.
(18) Veitch, N. C.; Williams, R. J. P. In *Biochemical, Molecular and Physiological Aspects of Plant Peroxidases*; Lobarzewski, J., Greppin, H., Penel, C., Gaspar, T., Eds.; University of Geneva: Geneva, 1991; pp 99−109.
(19) Banci, L.; Bertini, I.; Turano, P.; Ferrer, J. C.; Mauk, A. G. *Inorg. Chem.* **1991**, *30*, 4510−4516.
(20) Veitch, N. C.; Williams, R. J. P.; Bray, R. C.; Burke, J. F.; Sanders, S. A.; Thorneley, R. N. F.; Smith, A. T. *Eur. J. Biochem.* **1992**, *207*, 521−531.
(21) Veitch, N. C.; Williams, R. J. P.; Smith, A. T.; Sanders, S. A.; Thorneley, R. N. F.; Bray, R. C.; Burke, J. F. *Biochem. Soc. Trans.* **1992**, *20*, 114S.
(22) Sette, M.; de Ropp, J. S.; Hernández, G.; La Mar, G. N. *J. Am. Chem. Soc.* **1993**, *115*, 5237−5245.
(23) Chen, Z.; de Ropp, J. S.; Hernández, G.; La Mar, G. N. *J. Am. Chem. Soc.* **1994**, *116*, 8772−8783.
(24) de Ropp, J. S.; Chen, Z.; La Mar, G. N. *Biochemistry* **1995**, *34*, 13477−13484.
(25) La Mar, G. N.; Chen, Z.; Vyas, K.; McPherson, A. D. *J. Am. Chem. Soc.* **1995**, *117*, 411−419.
(26) Veitch, N. C.; Williams, R. J. P.; Bone, N. M.; Burke, J. F.; Smith, A. T. *Eur. J. Biochem.* **1995**, *233*, 650−658.
(27) Pierattelli, R.; Banci, L.; Turner, D. L. *J. Biol. Inorg. Chem.* **1996**, *1*, 320−329.
(28) de Ropp, J. S.; Mandal, P.; Brauer, S. L.; La Mar, G. N. *J. Am. Chem. Soc.* **1997**, *119*, 4732−4739.
(29) de Ropp, J. S.; Mandal, P.; La Mar, G. N. *Biochemistry* **1999**, *38*, 1077−1086.
(30) Gajhede, M.; Schuller, D. J.; Henriksen, A.; Smith, A. T.; Poulos, T. L. *Nat. Struct. Biol.* **1997**, *4*, 1032−1038.
(31) La Mar, G. N.; de Ropp, J. S. In *Biological Magnetic Resonance*; Berliner, L. J., Reuben, J., Eds.; Plenum Press: New York, 1993; Vol. 12, pp 1−78.
(32) Bertini, I.; Luchinat, C. *Coord. Chem. Rev.* **1996**, *150*, 1−296.
(33) La Mar, G. N.; Satterlee, J. D.; de Ropp, J. S. In *The Porphyrin Handbook*; Kadish, K. M., Smith, K. M., Guilard, R., Eds.; Academic Press: San Diego, 1999; Vol. 5, pp 185−298.
(34) Williams, G.; Clayden, N. J.; Moore, G. R.; Williams, R. J. P. *J. Mol. Biol.* **1985**, *183*, 447−460.
(35) Emerson, S. D.; La Mar, G. N. *Biochemistry* **1990**, *29*, 1556−1566.

anisotropies of the diagonal paramagnetic susceptibility tensor, χ. The magnetic axes and anisotropies provide valuable information on the coordination symmetry of the heme iron, while the geometric factors in eq 1 contain a wealth of unique structural information on the active site.[32,33,36,37] The magnetic anisotropy, which in high-spin iron is essentially axial ($\Delta\chi_{rh} \sim 0$) with the unique axis normal to the heme (i.e., $\beta = 0$ in Figure 1B), is given by:[32,38]

$$\Delta\chi_{ax} = -S(S+1)(2S-1)(2S+3)g^2\beta^2D(36k^2T^2)^{-1} \quad (2)$$

$\Delta\chi_{ax}$ provides important information on the effective axial field through the zero-field splitting parameter D, which gives insight into the nature of the His−Fe bond and the presence or absence of a ligated water molecule.[33,39−41] Combining eqs 1 and 2 with $Z = -S(S+1)(2S-1)(2S+3)g^2\beta^2(432\pi N_A k^2)^{-1}$, yields:

$$\delta_{dip} = (ZD/T^2)(3\cos^2\theta' - 1)R_{Fe}{}^{-3}\Gamma(\alpha,\beta,\gamma) \quad (3)$$

Because of its superior resolution and minimal paramagnetic relaxation, the most effective NMR studies of HRP to date have been carried out on the cyanide-inhibited enzyme, HRP-CN,[11,15,17−21,23,24,26,42] for which there is now also a very well-developed interpretative basis of the hyperfine shift in terms of active site electronic and molecular structure.[25,29] It is recognized that 2D NMR experiments are intrinsically less effective for high-spin than low-spin heme proteins.[31−33] However, *it is vital to explore the limits to NMR characterization of high-spin, resting state peroxidases because they are the physiologically relevant forms*. While contact shifts are much larger in HRP than in HRP-CN, they resolve resonances only for the heme and axial His, all of which have been previously assigned by both isotope labeling and 1D/2D NMR.[12,16,43,44] In general, the relaxation is ∼5−10 times greater but the magnetic anisotropy only ∼20% larger in high-spin HRP than low-spin HRP-CN. Therefore, the majority of the residues in contact with the heme (i.e., "first sphere") are much too strongly relaxed ($T_1 < 15$ ms for $R_{Fe} \leq 8$ Å), without being resolved, in HRP to characterize effectively by NMR.[28] However, since relaxation falls off as $R_{Fe}{}^{-6}$, while the dipolar shift falls off only as $R_{Fe}{}^{-3}$, there should be a region near the heme, namely the "second sphere" residues with 8 Å $\leq R_{Fe} \leq$ 15 Å, in which protons are not too seriously relaxed but yet experience significant dipolar shifts. While such residues only occasionally exhibit signals resolved from the diamagnetic envelope, the combination of the weak to moderate relaxation with dipolar shifts characteristic of high-spin heme iron allows their detection in appropriately tailored 2D NMR carried out over a range of temperatures to establish the uniqueness of scalar and/or dipolar connections.[39]

An important subset of target residues in this "second sphere" in HRP includes the aromatic residues whose mutation influences substrate binding.[9−11] Initial work on HRP had detected five unassigned aromatic spin systems, along with parts of three Leu/Val and one Ile spin system shifted upfield.[17] Subsequent work, using short mixing times and rapid repetition rates,[28] emphasized strongly relaxed resonances and located three aromatic residues in contact with the heme: Phe152 next to 3-CH_3, Phe172 next to 5-CH_3, and a Phe W, later identified as Phe179,[11] next to 8-CH_3. Here we again address resting state HRP by solution NMR, with emphasis on the less severely relaxed "second sphere" residues. Our goals are to explore the extent to which definitive assignment and structural characterization are achievable for high-spin heme enzymes, and to provide a quantitative interpretive basis of the dipolar shifts in terms of molecular structure and the zero-field splitting parameter D. It is recognized that comprehensive assignments will allow future NMR structural characterization of mutants for which crystallography is not practical. Subsequently, we extend the strategy to the H42A-HRP mutant to demonstrate that D is minimally reduced and dictates the retention of five coordination of the iron. An important component of our analysis is the use of predicted δ_{dip}, in eq 1, for target residues based on comparison with observed value, δ_{dip}(obs), given by

$$\delta_{dip}(obs) = \delta_{DSS}(obs) - \delta_{DSS}(dia) \quad (4)$$

Since many of the δ_{dip}(calc) from eq 3 are only a few tenths of a ppm, large uncertainties in δ_{DSS}(dia) can lead to highly inaccurate δ_{dip}(obs) estimates via eq 4. However, we have demonstrated that the temperature gradient, Gr ≡ d/d(T^{-2}), of the observed and calculated dipolar shifts obviates the need for δ_{DSS}(dia) and yields:[45,46]

$$\mathrm{Gr}[\delta_{dip}(obs)] = \mathrm{Gr}[\delta_{DSS}(obs)] - \mathrm{Gr}[\delta_{DSS}(dia)] \approx \mathrm{Gr}[\delta_{DSS}(obs)] \quad (5)$$

Combining eqs 3 and 5 yields:[45,46]

$$\mathrm{Gr}[\delta_{dip}(calc)] = ZD(3\cos^2\theta' - 1)\mathrm{R}_{Fe}{}^{-3}\Gamma(\alpha,\beta,\gamma) \quad (6)$$

if the molecular structure and magnetic axes are independent of temperature.[47]

Experimental Section

Proteins. Wild-type (WT) horseradish peroxidase isozyme C was purchased from Boehringer-Mannheim as a lyophilized salt free powder and used without further purification. Throughout this work the protein will be referred to as HRP without further reference to isozyme type. The sample concentration was 3 mM in 99.8% ^2H_2O. The N-terminal polyhistidine-tagged recombinant, rWT, HRP and H42A HRP were expressed and purified as previously described.[8] The rWT and H42A proteins include a 10 residue N-terminal polyhistidine tag for purification purposes.

NMR Spectroscopy. ^{1}H NMR spectra were collected in ^2H_2O solution on GE Ω-300 (300 MHz), Bruker AMX-400 (400 MHz), GE Ω-500 (500 MHz), and Bruker DRX-600 (600 MHz) spectrometers over the temperature range 25−55 °C for WT HRP and 25−30 °C for H42A-HRP. Data were obtained over the complete ±100 ppm bandwidth at a repetition rate of 20 s^{-1} and over the ±10 ppm window at a repetition rate of 1 s^{-1}. Nonselective T_1 values were determined from the slope of the initial recovery of the magnetization in an

(36) Bertini, I.; Turano, P.; Vila, A. J. *Chem. Rev.* **1993**, *93*, 2833−2933.
(37) Yamamoto, Y. *Ann. Rpt. NMR Spectrosc.* **1998**, *36*, 1−77.
(38) Kurland, R. J.; McGarvey, B. R. *J. Magn. Reson.* **1970**, *2*, 286−301.
(39) Clark, K.; Dugad, L. B.; Bartsch, R. G.; Cusanovich, M. A.; La Mar, G. N. *J. Am. Chem. Soc.* **1996**, *118*, 4654−4664.
(40) Rajarathnam, K.; La Mar, G. N.; Chiu, M. L.; Sligar, S. G.; Singh, J. P.; Smith, K. M. *J. Am. Chem. Soc.* **1991**, *113*, 7886−7892.
(41) Kao, Y. H.; Lecomte, J. T. J. *J. Am. Chem. Soc.* **1993**, *115*, 9754−9762.
(42) de Ropp, J. S.; Yu, L. P.; La Mar, G. N. *J. Biomol. NMR* **1991**, *1*, 175−190.
(43) Thanabal, V.; de Ropp, J. S.; La Mar, G. N. *J. Am. Chem. Soc.* **1987**, *109*, 265−272.
(44) de Ropp, J. S.; La Mar, G. N. *J. Am. Chem. Soc.* **1991**, *113*, 4348−4350.
(45) Xia, Z.; Nguyen, B. D.; La Mar, G. N. *J. Biomol. NMR* **2000**, *17*, 167−174.
(46) Baxter, N. J.; Williamson, M. P. *J. Biomol. NMR* **1997**, *9*, 359−369.
(47) Nguyen, B. D.; Xia, Z.; Yeh, D. C.; Vyas, K.; Deaguero, H.; La Mar, G. N. *J. Am. Chem. Soc.* **1999**, *121*, 208−217.

inversion−recovery experiment for resolved signals, or estimated from the null point for partially resolved signals and the differential relaxation analyzed in terms of the distance to the iron, R_{Fe}, via:[31,32]

$$T_1^{-1} \propto R_{Fe}^{-6} \tag{7}$$

Steady-state NOEs on H42A-HRP at 300 and 400 MHz were obtained by partially saturating the desired resolved low-field peak, as described in detail previously.[16] Clean-TOCSY[48] (mixing time 20 and 40 ms) and NOESY[49] spectra were recorded at 600 MHz over a bandwidth of ±10 ppm by using 2048 t_2 points and 512 t_1 blocks of 128−160 scans each collected at a repetition rate of 1 s^{-1}. NOESY data utilizing a range of mixing times from 30 to 200 ms were collected. The most effective data were collected with a mixing time of 65 ms, which approximates the mean relaxation time of the resonances of interest. The resulting 2D data sets were apodized by 30° to 45°-shifted sine-squared bell functions in both directions and zero-filled to 2048 × 2048 points prior to Fourier transformation. Data processing was carried out using Bruker Xwinnmr 2.5 software on a SGI O2 work station or MSI Felix 98 software on a SGI Indigo-2 work station.

Magnetic Axes. The anisotropy and orientation of the axially symmetric paramagnetic tensor were determined by a least-squares search for the minimum in the error function, F/n;[33−35]

$$F/n = \sum_{i=1}^{n} |\delta_{dip}(\text{obs}) - \delta_{dip}(\text{calc})|^2 \tag{8}$$

The δ_{dip}(calc) are given by eq 3, and the observed dipolar shifts are given by eq 4. The δ_{DSS}(dia) were estimated by two alternate routes. On one hand, the available crystal coordinates allow a calculation via the relation

$$\delta_{DSS}(\text{dia}) = \delta_{pep} + \delta_{sec} + \delta_{rc} \tag{9}$$

where δ_{pep} is the unfolded peptide shift[50] and δ_{sec} and δ_{rc} include the influence of secondary structure[51] and ring currents.[52] Alternatively, if eq 3 is valid as supported by available NMR data[28]

$$\delta_{DSS}(\text{dia}) = \delta_{int}(T^{-2}) \tag{10}$$

where $\delta_{int}(T^{-2})$ is the intercept, at $1/T^2 \rightarrow 0$, of a plot of δ_{DSS}(obs) vs T^{-2}. In either case, we use the HRP crystal coordinates[30] to calculate geometric factors in the reference coordinate system. Initially, it was assumed that the magnetic axis is normal to the heme (i.e., $\beta = 0$, so only $\Delta\chi_{ax}$ is determined). After making more assignments, the anisotropy and orientation of the axial tensor were redetermined allowing for tilt (β in degrees) of the axis from the heme normal in a direction defined by α in Figure 1A.

Results

The resolved low-field portions of resting state WT (rWT) and H42A-HRP proton spectra are illustrated in Figure 2. The chemical shifts of the rWT are essentially the same as those of WT, although the line widths are somewhat greater in the former, likely due to the additional poly-His tail on the protein.[8] The chemical shifts of WT and H42A HRP are listed in the Supporting Information.

Residue Assignment Strategy. Our target residues are ~50 amino acids with expected 30 ms ≤ T_1 < 180 ms and 0.2 ≤ $|\delta_{dip}|$ ≤ 2 ppm located 9−16 Å from the iron, whose relevant cross-peaks can be resolved in a 2D map. Residues expected to be particularly accessible to detection and assignment include aromatic side chains and their ring current and upfield dipolar shifted methyl-containing aliphatic contacts, and non-methyl-containing aliphatic protons that exhibit significant downfield dipolar shifts (i.e., $C_\alpha H$).[39] For simplicity we assign letter labels to previously unassigned TOCSY-detected fragments (or isolated signals), reserving upper case italic letters for aliphatic (*A*−*Z* followed by *A*′−*D*′) and lower case italic letters (*a*−*r*) for aromatic spin systems. (Note that a Phe contains an aromatic (C_6H_5) and an aliphatic ($C_\alpha HC_\beta H_2$) spin system.) Individual protons on a spin system prior to assignment are labeled by a number (e.g., *A1*). In each case, we initiate the sequential labeling of the aromatic system from the low-field side and the aliphatic system from the high-field side of the spectrum. Previously assigned peaks are given by their residue number and proton type.[11,28] Table 1 lists all peaks assigned herein as described below.

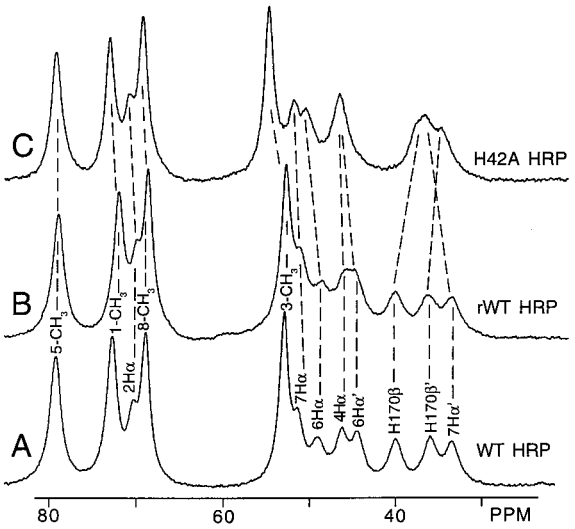

Figure 2. Comparison of the resolved low-field portions of the 300 MHz ^{1}H NMR spectra of high-spin ferric (A) WT, (B) rWT, and (C) H42A-HRP in ^2H_2O at pH 7.0 at 30 °C. The previously reported assignments[12,16,44] of WT are given, and the peaks assigned in the mutant are connected by dashed lines.

Five forms of NMR data provide the basis for the assignment of our target residues.[39] (i) Variable-temperature 1D/2D NMR spectra identify signals with a significant temperature dependence to their shift. A slope of 0.15 ppm·K^{-2} × 10^{-5} in a plot of δ_{DSS}(obs) vs T^{-2} reflects δ_{dip}(obs) ~0.2 ppm, and intercepts in a plot of δ_{DSS}(obs) vs T^{-2} yield δ_{DSS}(dia) via eq 10. δ_{DSS}(dia) can then indicate the functionality of the proton. (ii) TOCSY spectra over a range of temperatures provide limited but crucial (and occasionally complete) information on spin-topology of side chains (i.e. Val vs Leu vs Ile). (iii) Dipolar (NOESY) contacts to the heme, to assigned residues, and among unassigned residues are interpreted based on the prediction of the crystal structure.[30] (iv) Paramagnetic-induced dipolar relaxation[32,33] yields estimates of R_{Fe} via eq 7. (v) Last, but most importantly, use of Gr[δ_{dip}(obs)] in conjunction with the geometric factor ($3\cos^2\theta - 1)R^{-3}$ from the HRP crystal structure is used to predict dipolar shifts. The completed assignments are subsequently used to determine both the anisotropy and orientation of the paramagnetic susceptibility tensor.

Characterization of Side Chain Type. TOCSY spectra (not shown, all TOCSY spectra are given in the Supporting Information) detect the rings of 20 of the 26 (20 Phe, 5 Tyr, 1 Trp)

(48) Griesinger, C.; Otting, G.; Wüthrich, K.; Ernst, R. R. *J. Am. Chem. Soc.* **1988**, *110*, 7870−7872.
(49) Macura, S.; Ernst, R. R. *Mol. Phys.* **1980**, *41*, 95−117.
(50) Bundi, A.; Wüthrich, K. *Biopolymers* **1979**, *18*, 285−297.
(51) Wishart, D. S.; Sykes, B. D.; Richards, F. M. *J. Mol. Biol.* **1991**, *222*, 311−333.
(52) Cross, K. J.; Wright, P. E. *J. Magn. Reson.* **1985**, *64*, 240−231.

Table 1. ^{1}H NMR Spectral Parameters for Assigned Nonligated Residues in WT and H42A HRP

			WT HRP					H42A HRP
residue	symbol	proton	δ_{DSS}(obs)[a] at 55 °C	$\delta_{int}(T^{-2})$[b]	Gr[δ_{DSS}(obs)][c]	δ_{DSS}(dia)[d]	δ_{DSS}(obs)[e] at 30 °C	δ_{DSS}(obs)[f] at 30 °C
Phe45	*m1*	C_δH(?)	7.09	6.7	0.38	7.15	7.15	
	m2	C_ϵH(?)	7.09	6.7	0.38	7.20	7.15	
	m3	C_ζH(?)	5.98	5.9	0.13	5.04	6.00	
Phe61	*h1*	C_ϵH(?)	7.16	7.3	−0.19	7.27	7.13	7.13
	h2	C_ζH(?)	6.78	6.9	−0.13	7.22	6.76	6.78
Phe68	*d1*	C_ζH	7.67	7.4	0.25	7.36	7.71	
	d2	C_ϵH	7.58	7.5	0.13	7.42	7.60	7.57
	d3	C_δH	7.31	7.4	−0.13	7.33	7.29	7.32
Phe77	*n1*	C_δH	7.02	7.3	−0.25	7.24	6.98	6.99
	n2	C_ϵH	6.53	7.0	−0.56	7.28	6.44	6.50
	n3	C_ζH	6.02	6.7	−0.75	7.18	5.90	5.95
Phe130	*j1*	C_ζH	7.10	7.2	−0.13	7.20	7.08	7.08
	j2	C_ϵH	6.91	7.1	−0.19	7.26	6.88	6.89
	j3	C_δH	6.83	7.1	−0.31	7.17	6.78	6.79
Phe142	*X1*	$C_{\beta2}$H	3.77	3.4	0.38	3.17	3.83	3.78
	X2	$C_{\beta1}$H	4.34	3.8	0.63	3.20	4.44	4.36
	X3	C_αH	5.76	5.1	0.75	4.73	5.88	5.78
	a1	C_δH	8.16	7.7	0.50	7.61	8.24	8.21
	a2	C_ϵH	8.16	7.7	0.50	7.60	8.24	8.21
	a3	C_ζH	7.88	7.6	0.31	7.57	7.93	7.93
Phe143	*C′1*	$C_{\beta1}$H[g]	4.83			3.15		
	C′2	C_αH	5.43	4.8	0.69	4.63	5.54	5.45
	b1	C_ϵH	8.12	7.5	0.63	7.50	8.22	8.21
	b2	C_ζH	7.93	7.5	0.44	7.44	8.00	8.00
	b3	C_δH	7.91	7.3	0.66	7.37	8.01	8.00
Phe152	*D′1*	C_αH	4.88	4.5	0.44	4.45	4.95	4.92
		C_ζH	10.14	7.4	2.96	8.07	*h*	
		C_ϵH	9.33	7.5	1.94	7.98	9.64	9.31
		C_δH	8.67	7.8	0.94	7.73	8.82	8.80
Phe172		C_ζH	8.98	8.2	0.88	7.76	9.18	9.02
		C_ϵH	8.29	7.2	1.18	7.83	8.48	8.19
		C_δH	8.29	7.9	0.44	7.47	8.36	8.19
Phe179	*A′1*	$C_{\beta2}$H	4.73	3.5	1.38	3.23	4.95	4.75
	A′2	$C_{\beta1}$H	5.05	3.6	1.57	3.35	5.30	5.27
	A′3	C_αH	5.72	5.1	0.63	4.68	5.82	5.77
		C_δH	9.18	8.0	1.31	7.72	9.39	9.27
		C_ϵH	8.53	7.7	0.88	7.76	8.67	8.60
		C_ζH	8.00	7.4	0.69	7.61	8.11	8.11
Phe229	*r1*	C_δH	8.14[i]	7.6	0.44	6.94	8.16	
	r2	C_δH	8.08[i]	7.8	0.29	5.71	8.11	
	r3	C_ϵH	6.68[i]	6.2	0.44	6.45	6.71	
	r4	C_ϵH	6.52[i]	6.2	0.29	7.09	6.54	6.46
	r5	C_ζH	5.45[i]	5.5	0	4.88	5.45	5.31
Tyr234	*p1*	$C_{\delta1}$H	6.62	6.8	−0.19	7.03	6.59	6.63
	p2	$C_{\delta2}$H	6.28	6.8	−0.50	6.63	6.20	
	p3	$C_{\epsilon1}$H	6.11	6.6	−0.50	6.97	6.03	6.10
	p4	$C_{\epsilon2}$H	4.39	5.0	−0.69	4.44	4.28	
Phe251	*i1*	C_ζH	7.15	7.3	−0.19	7.27	7.12	7.15
	i2	C_ϵH	7.07	7.2	−0.19	7.31	7.04	7.05
	i3	C_δH	6.66	6. 9	−0.25	7.22	6.62	6.63
Phe266	*k1*	C_ζH	7.10	6.9	0.25	7.36	7.14	7.11
	k2	C_ϵH	7.01	7.1	−0.06	7.40	7.00	6.99
	k3	C_δH	6.38	6.5	−0.13	6.73	6.36	6.33
Phe273 or Phe274(?)	*c1*	C_δH	7.78	7.8	−0.06	6.95	7.77	7.76
	c2	C_ϵH	7.31	7.3	0	7.35	7.31	7.29
	c3	C_ζH	6.94	6.9	0	7.02	6.94	6.93
Phe277(?)	*q1*	C_ζH	8.78[i]	7.7	1.03	7.79	8.85	
	q2	C_ϵH	7.83[i]	7.2	0.59	7.66	7.87	
Leu39	*B1*	$C_{\delta2}H_3$	−0.72	0.3	−1.06	0.24	−0.89	−0.73
	B2	$C_{\delta1}H_3$	−0.28	0.0	−0.31	0.32	−0.33	−0.23
	B3	$C_{\beta2}$H[g]	0.32			1.48		
	B4	C_γH	1.06	1.4	−0.31	1.17	1.01	1.16
His/Ala42	*K1*	$C_{\beta1}$H	0.04	2.3	−2.38	1.97	−0.34	
		$C_\beta H_3$						−3.16
Asp43	*Z1*	C_αH	4.34	4.9	−0.63	4.27	4.24	4.44
Val46	*E1*	$C_{\gamma2}H_3$	−0.25	0.5	−0.75	0.65	−0.37	−0.31
	E2	$C_{\gamma1}H_3$	0.33	0.7	−0.44	0.85	0.26	0.26
	E3	C_βH	1.95	2.4	−0.44	1.94	1.88	1.82
	E4	C_αH	3.48	3.8	−0.31	3.97	3.43	3.44

Table 1 (Continued)

			WT HRP					H42A HRP
residue	symbol	proton	δ_{DSS}(obs)[a] at 55 °C	$\delta_{int}(T^{-2})$[b]	Gr[δ_{DSS}(obs)][c]	δ_{DSS}(dia)[d]	δ_{DSS}(obs)[e] at 30 °C	δ_{DSS}(obs)[f] at 30 °C
Ile53	*D1*	$C_{\delta1}H_3$	−0.56	0.8	−1.44	0.51	−0.79	−0.74
	D2	$C_{\gamma2}H_3$	−0.11	0.6	−0.75	0.69	−0.23	0.19
	D3	$C_{\gamma1}H$	0.35	1.1	−0.75	1.02	0.23	0.45
	D4	$C_{\gamma2}H$	0.43	1.2	−0.88	1.15	0.29	0.55
	D5	$C_{\beta}H$	1.01	2.0	−1.10	1.55	*h*	
	D6	$C_{\alpha}H$	3.30	3.8	−0.56	3.96	3.21	3.29
Leu54(?)	*N1*	$C_{\delta2}H_3$	0.50	0.8	−0.33	0.86	*h*	
	N2	$C_{\delta1}H_3$	0.59	0.8	−0.25	0.73	0.55	0.57
Leu55	*M1*	$C_{\delta1}H_3$	0.12	0.4	−0.25	0.50	0.08	0.07
	M2	$C_{\delta2}H_3$	0.45	0.6	−0.19	0.74	0.42	0.42
Ala74	*L1*	$C_{\beta}H_3$	0.09	1.1	−1.06	1.19	−0.08	
	L2	$C_{\alpha}H$	2.94	3.8	−0.94	3.89	2.79	
Ala112	*V1*	$C_{\beta}H_3$	2.18	1.7	0.56	1.67	2.27	2.11
	V2	$C_{\alpha}H$	5.01	4.8	0.19	4.37	5.04	5.02
Ala134	*P1*	$C_{\beta}H_3$	0.65	1.3	−0.69	1.19	0.54	0.63
	P2	$C_{\alpha}H$	3.30	3.9	−0.69	3.87	3.19	3.31
Leu138		$C_{\delta2}H_3$	−2.49	−0.6	−2.00	−0.31	−2.81	−2.68
		$C_{\delta1}H_3$	−2.18	−0.2	−2.13	−0.15	−2.52	−1.67
		$C_{\beta1}H$	−1.54	0.5	−2.19	0.90	−1.89	
		$C_{\beta2}H$	0.55	1.4	−0.94	1.29	0.40	
		$C_{\gamma}H$	0.19	1.0	−0.81	1.10	0.06	0.11
		$C_{\alpha}H$	3.30	3.8	−0.56	3.98	3.21	
Ala140	*R1*	$C_{\beta}H_3$	1.30	0.6	0.75	0.55	1.42	1.34
Ser151	*B′1*	$C_{\alpha}H$	4.76	4.5	0.31	4.50	4.81	4.82
	B′2	$C_{\beta1}H$	5.16	4.4	0.88	4.52	5.30	5.19
	B′3	$C_{\beta2}H$	5.10	4.4	0.63	4.40	5.20	5.28
Val155	*J1*	$C_{\gamma2}H_3$	−0.05	0.1	−0.13	−0.35	−0.07	0.05
	J2	$C_{\gamma1}H_3$	0.48	0.4	0.06	0.39	0.49	0.57
	J3	$C_{\beta}H$	2.11	2.0	0.13	1.59	2.13	2.17
	J4	$C_{\alpha}H$	4.39	4.3	0.13	3.39	4.41	4.43
Leu157	*Q1*	$C_{\delta1}H_3$	1.20	0.7	0.56	0.98	1.29	1.23
Val164(?)	*H1*	$C_{\gamma2}H_3$	−0.11	0.5	−0.63	0.87	−0.21	−0.15
	H2	$C_{\gamma1}H_3$	0.08	0.6	−0.50	1.00	0.00	0.03
Gln176	*W1*	$C_{\beta2}H$	2.87	2.2	0.69	2.36	2.98	2.92
	W2	$C_{\beta1}H$	3.23	2.5	0.75	2.08	3.35	3.29
	W3	$C_{\alpha}H$	5.61	5.2	0.44	4.44	5.68	5.65
Ser216	*Y1*	$C_{\beta2}H$	4.02	3.8	0.25	3.93	4.06	4.02
	Y2	$C_{\beta1}H$	4.27	4.0	0.25	3.95	4.31	4.26
	Y3	$C_{\alpha}H$	5.56	4.9	0.69	4.43	5.67	5.58
Leu218	*T1*	$C_{\delta2}H_3$	1.55	0.8	0.81	0.96	1.68	1.60
Thr227	*S1*	$C_{\gamma2}H_3$	1.42	1.2	0.25	1.29	1.46	1.43
	S2	$C_{\beta}H$	4.96	4.6	0.38	4.38	5.02	5.00
	S3	$C_{\alpha}H$	5.34	4.5	0.94	4.60	5.49	5.48
Leu237	*A1*	$C_{\delta2}H_3$	−1.11	0.1	−1.25	0.10	−1.31	−1.21
	A2	$C_{\delta1}H_3$	−0.50	0.2	−0.75	0.39	−0.62	−0.54
	A3	$C_{\gamma}H$	0.23	0.9	−0.75	0.43	0.11	0.24
	A4	$C_{\beta2}H$	0.96	1. 7	−0.77	1.15	*h*	
	A5	$C_{\alpha}H$	3.17	3.7	−0.56	3.95	3.08	3.21
Gly242	*U1*	$C_{\alpha2}H$	1.81	2.9	−1.18	3.55	1.63	1.77
	U2	$C_{\alpha1}H$	2.34	3.4	−1.18	3.60	2.16	2.34
Leu243	*C1*	$C_{\delta2}H_3$	−0.66	0.1	−0.77	0.03	*h*	
	C2	$C_{\delta1}H_3$	0.23	0.7	−0.55	0.49	*h*	
	C3	$C_{\gamma}H$[g]	0.39			1.25		
Asp247	*G1*	$C_{\beta1}H$	−0.20	2.0	−2.41	2.36	*h*	
Leu250	*F1*	$C_{\delta2}H_3$	−0.22	0.1	−0.38	0.74	−0.28	−0.25
	F2	$C_{\delta1}H_3$	0.19	0.4	−0.25	0.72	0.15	0.20
	F3	$C_{\gamma}H$	0.56	0.9	−0.31	1.57	0.51	
Val263	*O1*	$C_{\gamma2}H_3$	0.53	0.7	−0.13	0.92	0.51	0.41
	O2	$C_{\gamma1}H_3$	0.68	0.9	−0.19	0.79	0.65	0.53
	O3	$C_{\beta}H$	2.23	2.3	−0.06	2.16	2.22	2.23
	O4	$C_{\alpha}H$	2.84	3.0	−0.19	3.40	2.81	2.81

[a] Observed chemical shift at 55 °C in ppm, referenced to DSS. [b] Extrapolated intercept at $1/T^{-2} \rightarrow 0$, in ppm, of plot of observed chemical shift vs T^{-2}. [c] Temperature gradient of dipolar shift in ppm/K^{-2} as slope in a plot of δ_{DSS}(obs) vs T^{-2}. [d] Diamagnetic shift calculated on the basis of eq 9 and the crystal coordinates.[27] [e] Observed chemical shift for WT HRP at 30 °C in ppm, referenced to DSS. [f] Observed chemical shift for H42A HRP at 30 °C in ppm, referenced to DSS. [g] Peak detected only at 55 °C. [h] Peak not detected at 30 °C (gradient determined from data at 55 and 40 °C). [i] Observed chemical shift at 40 °C in ppm, referenced to DSS (resonance not resolved at 55 °C).

aromatic side chains[53] in the 5−10 ppm spectral window. Five aromatic rings exhibit downfield δ_{dip} (three with large δ_{dip}: Phe 152, Phe 172, Phe 179, and two with modest δ_{dip}: *a*, *b*) and three exhibit upfield δ_{dip} (*i*, *n*, *p*). The labeling scheme and shift data are presented in Table 1. Several aromatic spin systems show one or more protons shifted upfield by diamagnetic (likely

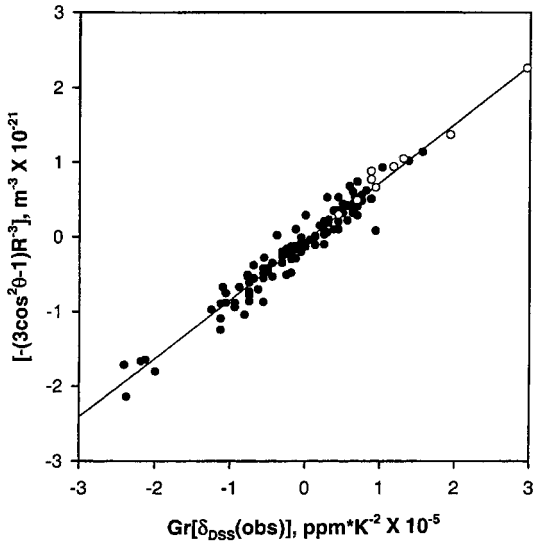

Figure 3. Plot of $d[\delta_{DSS}(obs)]/d[T^{-2}]$ vs $(3\cos^2\theta - 1)R^{-3}\Gamma(\alpha,\beta,\gamma)$ for HRP at 55 °C on the basis of the magnetic axis normal to the heme ($\Gamma(\alpha,\beta,\gamma) = 1$) for all assigned residue protons. The open circles represent the previously assigned Phe152, 172, and 179 ring protons.[11,28] Closed circles represent the remainder of definitely assigned resonances.

ring current) rather than dipolar shift, as $Gr[\delta_{DSS}(obs)]$ is small (Table 1). The 1 to −3 ppm spectral window reveals 11 aliphatic TOCSY-detected fragments with upfield δ_{dip}: three complete Val, one complete Leu, four Leu/Val (i.e. $(CH_3)_2CH$ fragments), one complete Ile, and two complete Ala. TOCSY spectra identify numerous fragments which contain downfield shifted $C_\alpha H$, including one two-spin $C_\alpha H-C_\beta H$, three three-spin $C_\alpha HC_\beta H_2$ fragments, a $C_\alpha H-C_\beta H-C_\gamma H$ fragment, two obvious Ser, and one Ala.

Heme Contacts. Saturation of assigned heme methyl peaks had previously yielded NOEs to the ring protons of three relaxed and dipolar shifted Phe, two of which could be assigned to Phe152 (near the heme 3-CH_3, 2-vinyl) and Phe172 (near 5-CH_3).[28] A third Phe ring was found near 8-CH_3 and later assigned to Phe179.[11] None of the other heme contact protons exhibited TOCSY connections, even in suitably tailored 2D, because of the expected strong relaxation.[28] With no further assignments possible via dipolar contacts to the heme, the alternate assignment strategy outlined above was followed. As a starting point, from a comparison of eqs 5 and 6, it is evident that a plot of $Gr[\delta_{DSS}(obs)]$ vs $(3\cos^2\theta' - 1)R^{-3}$ (utilizing the HRP crystal coordinates) should be linear. This was confirmed by the excellent correlation for the previously assigned[11,28] and significantly shifted Phe152, Phe 172, and Phe179 aromatic ring protons (open circles) plotted in Figure 3. Therefore candidates for further assignment were guided by the comparison of $(3\cos^2\theta' - 1)R^{-3}$ calculated for the target residues with the observed $Gr[\delta_{DSS}(obs)]$ presented in Table 1. Three regions of the "second sphere" of residues in HRP are addressed below: the substrate-binding pocket near pyrrole D (which is largely peripheral to the heme),[54] the pyrrole A/B junction extending to the distal pocket, and a cluster of aromatic residues in the vicinity of the proximal His 170.

(53) Table 1 provides labels and assignments for 16 aromatic side chains, consisting of 15 Phe and 1 Tyr. Three additional two-spin aromatic systems, Tyr or Phe with one spin not resolved, are observed in TOCSY (not shown, see Supporting Information) but not assigned. Two aromatic rings, Phe41 and Phe221, are too close to the iron to be observed in resting state HRP. We infer that four additional aromatic systems, including the single Trp, are not resolved or observed under the present conditions.

(54) Henriksen, A.; Schuller, D. J.; Meno, K.; Welinder, K. G.; Smith, A. T.; Gajhede, M. *Biochemistry* **1998**, *37*, 8054−8060.

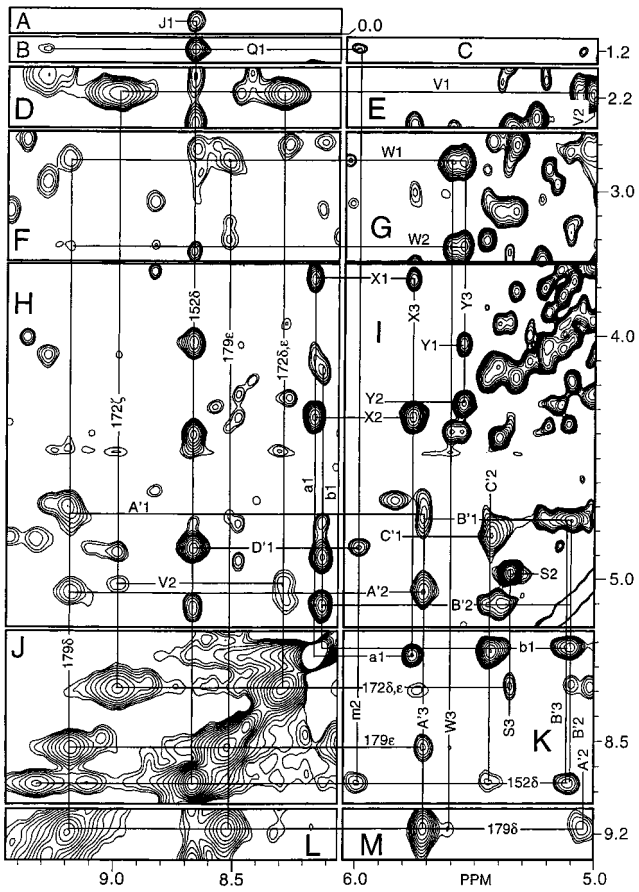

Figure 4. Portions of the 600 MHz NOESY spectra (mixing time 65 ms) of HRP illustrating dipolar contacts for moderately to strongly relaxed aromatic rings Phe *a* (Phe142), Phe *b* (Phe143), Phe152, Phe172, and Phe179. Portions A−I, K, and M are downfield shifted aliphatic contacts to these rings, and portions J and K are intra- and interring contacts.

The Substrate-Binding Pocket. Mutation of either Phe 68, Phe142, or Phe179 has been shown to affect the binding of the model substrate, benzhydroxamic acid, BHA.[11,26] Direct dipolar contact between BHA and the rings of Phe68 and Phe179, as well as to His42 and Ala 140, has been demonstrated for the BHA:HRP−CN complex.[18,29,55] The BHA:HRP crystal structure reveals additional contacts of the BHA with Arg38, His42, Pro139, Pro141, and Gly69,[54] of which all but Gly69 are much too strongly relaxed to detect in resting state HRP.[28] An additional residue near the substrate is Leu138. A strongly low-field shifted AMX spin system (*A′*) with very strong $C_\alpha H$ dipolar contact to the Phe179 $C_\delta H$ (Figures 4H, 4M) locates the Phe179 backbone. A similarly shifted $C_\alpha H-C_\beta H_2$ fragment *W* (Figure 4G) exhibits only very weak $C_\alpha H$ (Figure 4M), but strong $C_\beta H$, dipolar contacts (Figure 4F) to the Phe179 ring, as expected only for Gln176. Another low-field shifted AMX spin system, *Y*, with diamagnetic intercepts in the ∼4−5 ppm spectral window and a strong $C_\alpha H$ NOE to the Gln176 $C_\beta Hs$ (Figure 4G), locates Ser216. A weak NOE from the Phe179 ring to the ring of a moderately low-field shifted Arom *a*[56] (not shown) is consistent only with Arom *a* as Phe142. Intensities allow the individual assignment of the ring protons of F142 (not shown).

(55) La Mar, G. N.; Hernández, G.; de Ropp, J. S. *Biochemistry* **1992**, *31*, 9158−9168.

(56) The aromatic spin systems *a* and *b* when first observed were labeled as a single aromatic spin system "A".[17] From "A" NOEs were observed to another aromatic spin system originally labeled "D".[17] Here NOEs are observed from *d* to *a* and not to *b* (not shown; see Supporting Information).

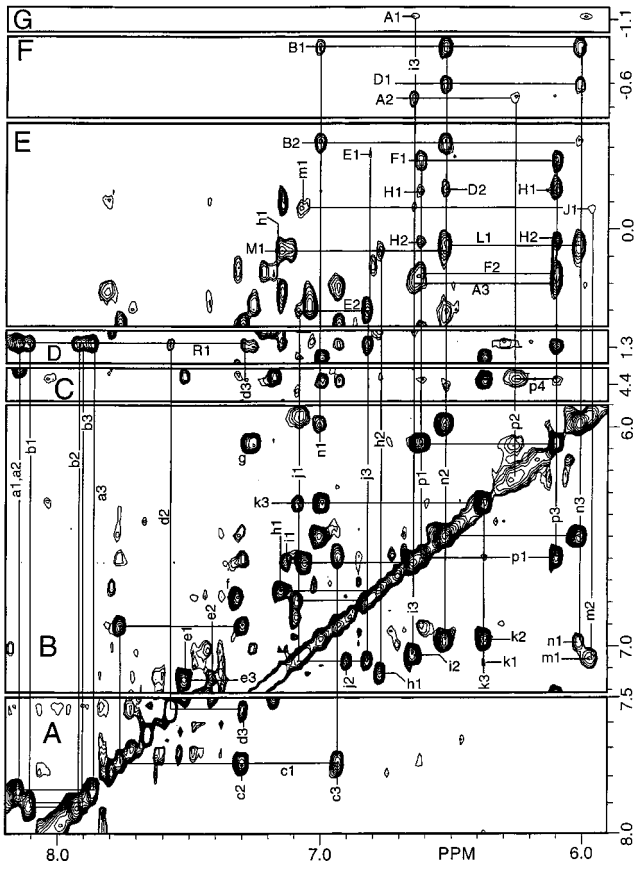

Figure 5. Portions of the 600 MHz NOESY spectrum (mixing time 65 ms) of HRP at 55 °C illustrating intra- and interring contacts (A−C) for weakly or moderately relaxed aromatic rings and their upfield-shifted aliphatic proton contacts (D−G).

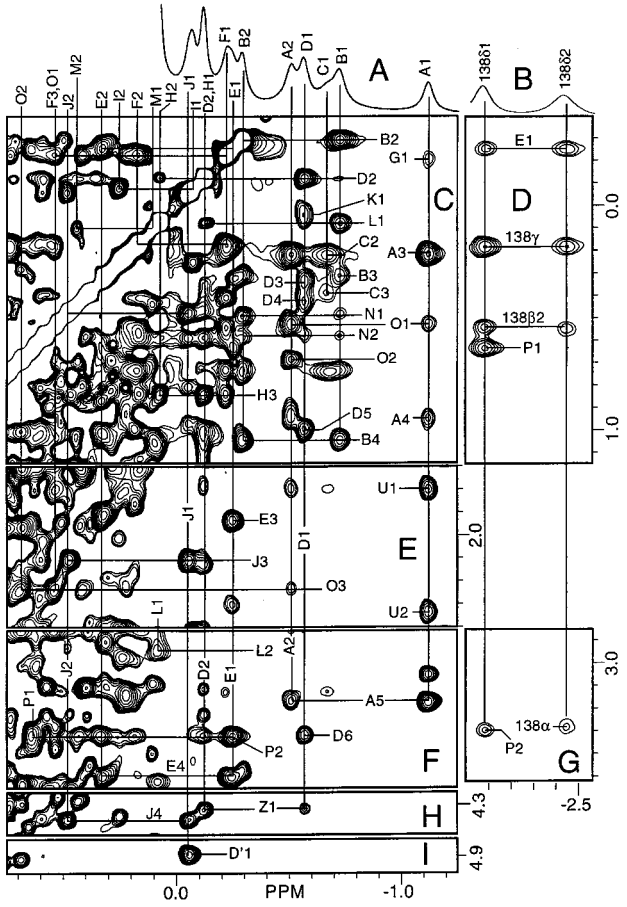

Figure 6. (A, B) Resolved upfield portions of the 600 MHz ^{1}H NMR reference spectrum of HRP at 55 °C and (C−I) portions of the NOESY spectrum (mixing time 65 ms) depicting the inter- and intraresidue contacts among these residues.

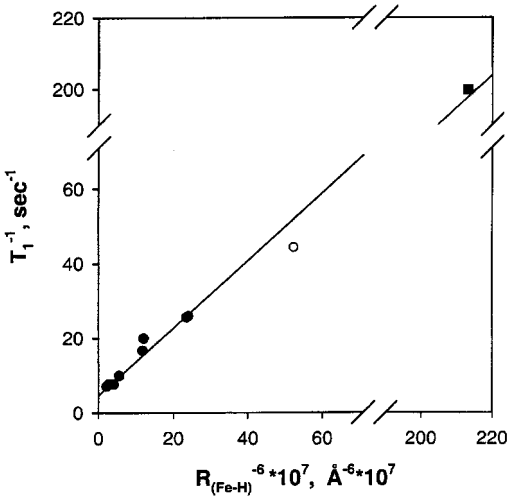

Figure 7. Plot of observed T_1^{-1} versus R^{-6} (determined from the HRP crystal structure) for resolved protons on nonligated residues of WT HRP (L39 $C_{\delta 1}H_3$, L39 $C_{\delta 2}H_3$, I53 $C_\delta H_3$, L138 $C_{\beta 1}H$, L138 $C_{\delta 1}H_3$, L138 $C_{\delta 2}H_3$, L237 $C_{\delta 1}H_3$, L237 $C_{\delta 2}H_3$, L243 $C_{\delta 2}H_3$, closed circles), Ala42 $C_\beta H_3$ in H42A HRP (open circle), and the heme methyls in WT HRP (closed square).

Strong NOESY cross-peaks to the ring $C_\delta H$ (*a1*) of Phe142 from a low-field shifted AMX spin system *X* identify the Phe142 backbone, Figure 4H, 4K. Gly69 is not strongly relaxed (R_{Fe} ∼9−10 Å), but the C_αHs are both shifted into the intractable 1−5 ppm window. Figure 1 schematically presents the observed NOESY contacts.

The previously assigned[28] Phe152 ring leads to assignment of both Leu138 and Phe143. First, the rings of Arom *b*[56] and Phe152 exhibit common NOESY cross-peaks to a TOCSY-connected AMX system *B*′ in the 4.5−5.2 ppm window (Figure 4K) with intercepts in the 4.5 to 4.0 ppm region (Table 1), which identifies *B*′ as Ser151 and Arom *b* as the ring of Phe143. NOESY cross-peaks for the low-field shifted CHCH spin system *C*′ to the ring $C_\delta H$ identify the Phe143 $C_\alpha HC_\beta H$ (Figure 4I) fragment; the other $C_\beta H$ was not assigned. A weak NOE from *C*′*2* ($C_\beta H$) to F152 $C_\delta H$ is also observed (Figure 4K) and confirms both assignments. The ring protons of Arom *m* exhibit NOESY cross-peaks to both the $C_\delta H$ (Figure 4K) and $C_\epsilon H$ (not shown) of Phe152 that are diagnostic of Phe45. A $C_\alpha H$ proton *D*′ exhibits strong NOEs to the Phe152 $C_\delta H$ and ring of Phe45 (Figure 4H,I) that are expected only for the Phe152 $C_\alpha H$; the $C_\beta H$s could not be definitely identified. Common NOESY cross-peaks to the methyls of a Val *J* by the Phe45 (Figure 5E) and Phe152 (Figure 4A) ring protons identify Val155, for which the upfield methyl exhibits the expected strong NOE to the Phe152 $C_\alpha H$ peak *D*′ (Figure 6I). Two resolved and strongly upfield shifted methyls (Figure 6B), which have been previously characterized[28] by TOCSY and assigned to Leu138, exhibit the expected weak NOE to the Phe45 ring (not shown), confirming both assignments. The Leu138 methyls exhibit T_1 values of 39, 60 ms for R_{Fe} 9.3, and 10.0 Å, respectively; the excellent correlation of observed relaxation rate with R_{Fe} is included in Figure 7.

The Phe142(*a*) ring protons exhibit moderate intensity NOESY cross-peaks to two ring protons of Arom *d*[56] (not

shown, see the Supporting Information), which exhibit negligible δ_{dip}; the only candidate is Phe68. Moreover, the ring protons of Phe142(*a*), Phe143(*b*), and Phe68(*d*) each exhibit NOESY cross-peaks to a low-field shifted methyl *R1* at 1.3 ppm (Figure 5D), as predicted only for the methyl of Ala140. The expected Ala140 $C_\beta H_3$-$C_\alpha H$ TOCSY cross-peak was not observed, likely because of the close proximity of the $C_\alpha H$ to the iron ($R_{Fe} \sim 8$ Å). The expected positions relative to the heme and the observed dipolar contacts of the substrate binding pocket residues are shown schematically in Figure 1. The plot of the correlation between Gr[δ_{DSS}(obs)] and δ_{dip}(calc) is given in Figure 3.

The Pyrrole A/B Junction and Distal Pocket. Numerous relaxed and dipolar-shifted methyl peaks are resolved or partially resolved in the upfield shoulder of the diamagnetic envelope, as shown at 55 °C in Figure 6A,B. TOCSY identifies a complete Ile *D* and the majority of a Leu *B*, each of which is relaxed and dipolar-shifted and which exhibit intraresidue NOESY cross-peaks (Figure 6C), as well as multiple NOESY cross-peaks to a three-spin, upfield shifted Phe *n* (Figure 5E,F). The arrangement of three such residues is unique in the HRP structure for Leu39, Ile53, and Phe77. The Ile53 $C_\delta H_3$ exhibits the expected weak NOE to $C_{\delta 1}H_3$ of Leu138 (not shown; see the Supporting Information). The Ile53 methyls exhibit prominent NOEs to a strongly upfield-shifted $C_\alpha H$ peak *Z1* (Figure 6H) that can only arise from Asp43. The methyls of a complete, upfield-shifted Val *E* exhibit NOESY cross-peaks to both Leu138 methyls (Figure 6D) and the $C_\alpha H$ of an Ala *P* (Figure 6F) which, in turn, is in contact with Leu138 $C_{\delta 1}H_3$ (Figure 6G), identifying Val46(*E*) and Ala134(*P*). A weakly upfield-shifted Phe *j* (Figure 5B) with NOESY cross-peaks to the Val46(*E*) methyls (Figure 5E) must arise from Phe130. An additional Ala *L* exhibits NOESY cross-peaks to both Ile53 $C_\delta H_3$(*D1*) (Figure 6C) and Phe77(*n*) (Figure 5E), and must arise from Ala74. The stereospecific assignment of the two Leu39 methyl groups was effected on the basis of their differential T_1 values. The Phe77(*n*) ring protons could be specifically assigned on the basis of the predicted NOE pattern to Leu39(*B*), and the assignments are confirmed by the predicted differential δ_{dip} values.

The crystal structure places the Ile53 $C_\delta H_3$(*D1*) only ~2.5 Å from the distal His42 $C_{\beta 1}H$. The latter proton has predicted $T_1 \sim 50$ ms ($R_{Fe} = 9.7$ Å) and δ_{dip}(calc) ~ 2 ppm. A NOESY cross-peak for Ile53 $C_\delta H_3$ to a relaxed and strongly upfield shifted proton *K1* (Figure 6C), which exhibits no further NOESY contacts, is assigned to His42 $C_{\beta 1}H$. The geminal $C_{\beta 2}H$ is too relaxed ($R_{Fe} = 8.8$ Å) to detect. The characteristic Ile53 contact with the residue 42 C_βHs can also be observed in the H42A-HRP mutant (see below). For the cases where T_1 values can be estimated for resolved (Figure 6B) or partially resolved (Figure 6A) upfield resonances, the correlation with R_{Fe}^{-6} is very good (Figure 7). The correlation of Gr(δ_{DSS}(obs)) in Table 1 with $(3\cos^2\theta' - 1)R^{-3}$ for assigned protons is excellent (Figure 3).

The Proximal Side and the Aromatic Cluster. Two relaxed, resolved, and upfield-shifted methyls *A1* and *A2* (Figure 6A) are traced by TOCSY (not shown; see the Supplementary Information) to a Leu *A* whose relaxation and δ_{dip} are those uniquely predicted for Leu237. A very weak NOE (not shown) to the upfield (predicted to be $C_{\delta 2}H_3$) Leu237 methyl upon saturating the previously assigned, low-field His170 C_βHs[14] is consistent with the assignment. The Leu 237 methyl T_1 values correlate well with R^{-6} (Figure 7). Strong NOESY cross-peaks between Leu237 $C_{\delta 2}H_3$ (*A1*) and a strongly TOCSY and NOESY spin-coupled pair of C_αHs of residue *U* with significant upfield δ_{dip} uniquely assign Gly242 (Figure 6E). A partially resolved, strongly relaxed and strongly upfield-shifted proton *G1*, which fails to exhibit any TOCSY cross-peaks, exhibits a NOE to the Leu237 $C_{\delta 2}H_3$ (*A1*), Figure 6C. The only relevant close contact predicted by the crystal structure to Leu 237 $C_{\delta 2}H_3$ is from $C_{\beta 1}H$ of Asp247, with predicted $\delta_{dip} \sim -2$ ppm and estimated $T_1 \sim 50$ ms ($R_{Fe} = 9.6$ Å). These data argue for the assignment of proton *G1* to Asp247 $C_{\beta 1}H$. The observed temperature gradient correlates reasonably well with the calculated geometric factor (Figure 3).

The Leu237 $C_\delta H_3$s (*A1*, *A2*) also exhibit NOESY cross-peaks to the ring protons of a negligibly dipolar shifted three-spin Arom *i* and an upfield dipolar shifted four-spin Arom *p* (Figures 5F, 5G), as well as to the methyls of TOCSY-detected Val *O* (not shown). This Val *O*, in turn, exhibits $C_\alpha H$ cross-peaks to the rings of negligibly dipolar shifted three-spin Arom *k* as well as Arom *p*, and a $C_\beta H$ contact to three-spin Arom *i* (not shown). The NOESY (Figure 5B) and TOCSY (not shown; see the Supporting Information) patterns for Arom *i* and *k* are consistent with those of rapidly reorienting Phe rings. The Arom *p* ring properties reflect a Tyr with a slowly reorienting ring for which the rate of rotation causes magnetization transfer[57] between the pairs of spin-coupled protons (Figure 5B,C). This pattern of dipolar shifts and dipolar contacts is consistent only with the assignment of Val263(*O*), a slowly reorienting Tyr234(*p*) ring and rapidly reorienting Phe251(*i*) and Phe266(*k*) rings, with the contacts summarized in Figure 1B. A very strong upfield ~2 ppm *diamagnetic* bias by ring current shift is predicted, and observed (Figure 5C), for the Tyr 234 $C_{\epsilon 2}H$ peak *p4*. The methyls of an isopropyl fragment *F* that exhibit cross-peaks to Tyr234(*p*) (Figure 5E), but not to Val263 (*O*), likely arise from Leu250(*F*). A partially resolved, upfield-shifted and strongly relaxed ($T_1 \sim 50$ ms) methyl *C1* exhibits two weak TOCSY (not shown; see the Supporting Information) and NOESY cross-peaks (Figure 6C), one of which is to an apparent moderately relaxed methyl at 0.23 ppm. The strong upfield-shift and relaxation uniquely identify *C1* as the Leu243 $C_{\delta 2}H_3$, $R_{Fe} = 9.9$ Å, with the two spin-coupled protons assigned as the $C_{\delta 1}H_3$ and $C_\gamma H$. This fragment failed to exhibit NOESY cross-peaks to any other assigned residue. The assigned residues and their diagnostic relation to the heme and each other are summarized in Figure 1, and the shift data are listed in Table 1.

The proximal aromatic cluster consists of two Tyr (233 and 234) and six Phe (229, 251, 266, 273, 274, and 277), of which three residues, Tyr234, Phe251, and Phe 266, are assigned above. The assignment of the remainder of the cluster is complicated by extensive line broadening of several rings due to ring reorientation in the intermediate NMR exchange time at 55 °C. However, the predicted δ_{rc}(diamagnetic) and δ_{dip}(calc) provide the following reasonable assignments. Arom *r* = Phe229, Arom *c* = Phe273 or 274, and Arom *q* = Phe 277, of which Phe 229 and Phe 277 exhibit slow reorientation of the rings. Details of the arguments appear in the Supporting Information. Since among this group only Phe229 and Phe277 are predicted to exhibit detectable δ_{dip}, and their magnitudes are relatively small, the cluster assignments are neither aided by δ_{dip} nor influence the magnetic axes deduced from δ_{dip}(obs).

Determination of the Magnetic Axes. The plot of Gr{δ_{DSS}(obs)] vs $(3\cos^2\theta - 1)R^{-3}$ exhibits a very good correlation based on the assumption of an axially symmetric χ oriented normal to the heme (Figure 3), which dictates that eq 2, and hence eq 3, are valid. Determining $\Delta\chi_{ax}$ via the one-parameter ($\Delta\chi_{ax}$) minimization of the error function in eq 8 yields $\Delta\chi_{ax} = (-2.61 \pm 0.11) \times 10^{-8}$ m^3/mol when using

(57) Sandström, J. *Dynamic NMR Spectroscopy*; Academic Press: New York, 1982.

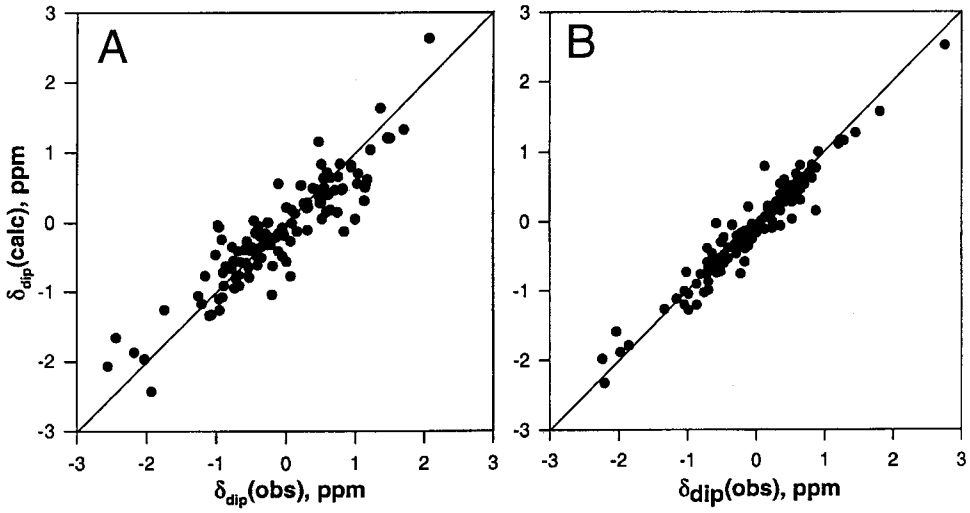

Figure 8. Plot of δ_{dip}(obs) versus δ_{dip}(calc) for assigned residues from a one-parameter search for $\Delta\chi_{ax}$ for WT HRP at 55 °C with (A) δ_{dip}(obs) determined by eqs 4 and 9 with $\Delta\chi_{ax} = -2.61 \times 10^{-8}$ m^3/mol and (B) δ_{dip}(obs) determined by eqs 4 and 10 with resulting $\Delta\chi_{ax} = -2.50 \times 10^{-8}$ m^3/mol. The straight line of unit slope represents a perfect fit.

eqs 4 and 9 to obtain δ_{dip}(obs), and $-2.50 \pm 0.07 \times 10^{-8}$ m^3/mol when using eqs 4 and 10. The resulting correlations are shown in Figure 8, parts A and B, respectively. *The correlation in Figure 8B, derived from using chemical shift gradients to obtain δ_{dip}(obs) via $\delta_{int}(T^{-2})$, is clearly superior*, although the $\Delta\chi_{ax}$ values are essentially the same. The extension of the searches to three parameters to determine α, β, and $\Delta\chi_{ax}$ yielded $\Delta\chi_{ax} = (-2.61 \pm 0.12) \times 10^{-8}$ m^3/mol, $\alpha = 46 \pm 50°$ and $\beta = 1 \pm 2°$, using eqs 4 and 9 to obtain δ_{dip}(obs), and $\Delta\chi_{ax} = (-2.51 \pm 0.06) \times 10^{-8}$ m^3/mol, $\alpha = -20 \pm 50°$, and $\beta = 2 \pm 1°$, using eqs 4 and 10, i.e., from chemical shift gradients.[58] The extension to three parameters thus leaves $\Delta\chi_{ax}$ essentially unchanged, leaves β near zero, and confirms a major magnetic axis oriented normal to the heme. The excellent correlations between δ_{dip}(obs) and δ_{dip}(calc) are shown in the Supporting Information.

His42Ala HRP. As the temperature of the WT HRP sample is lowered from 55 °C, there is a progressive loss of TOCSY cross-peaks due to the inevitable line broadening of most resonances, although a few aromatic residues which exhibit nonaveraged ring proton signals actually show narrower lines. However, the pattern of the *diagnostic intra- and interresidue NOESY cross-peaks* for the majority of assigned residues, and in particular, those with significant δ_{dip}, are still readily recognized in the NOESY map of WT HRP at 30 °C (not shown; see the Supporting Information). The diagnostic pattern of NOESY cross-peaks within the sets Leu237/Gly242/Tyr234/Phe251/Leu250, Phe68/Phe142/Phe143/Phe152/Val155/Ala140, and Leu39/Asp43/Val46/Ile53/Phe77/A134/Leu138, is particularly readily identified. The low-field portion of the ^{1}H NMR spectrum of H42A-HRP at 30 °C in Figure 2C can be compared to that of WT HRP at 30 °C in Figure 2B. The assignments for resolved low-field signals, determined by steady-state NOEs (not shown), are connected by dashed lines to the same assignments made previously in WT HRP.[12,14,16] Essentially the same pattern of shifts is found in the two proteins. The chemical shifts are listed in the Supporting Information.

The upfield resolved portion of the ^{1}H NMR spectrum of H42A-HRP is shown in Figure 9A and the NOESY contacts among aliphatic residues are shown in Figure 9B−D. The NOESY spectra involving dipolar contacts among aromatic rings, and between aromatic rings and the upfield-shifted aliphatic residues, are shown in Figure 10. The residues are labeled the same as for WT HRP in Figures 4−6 at 55 °C (and in the Supporting Information at 30 °C), and comparison of the chemical shifts at 30 °C of the WT and H42A proteins is shown in the last two columns of Table 1. The Phe152, Phe172, and

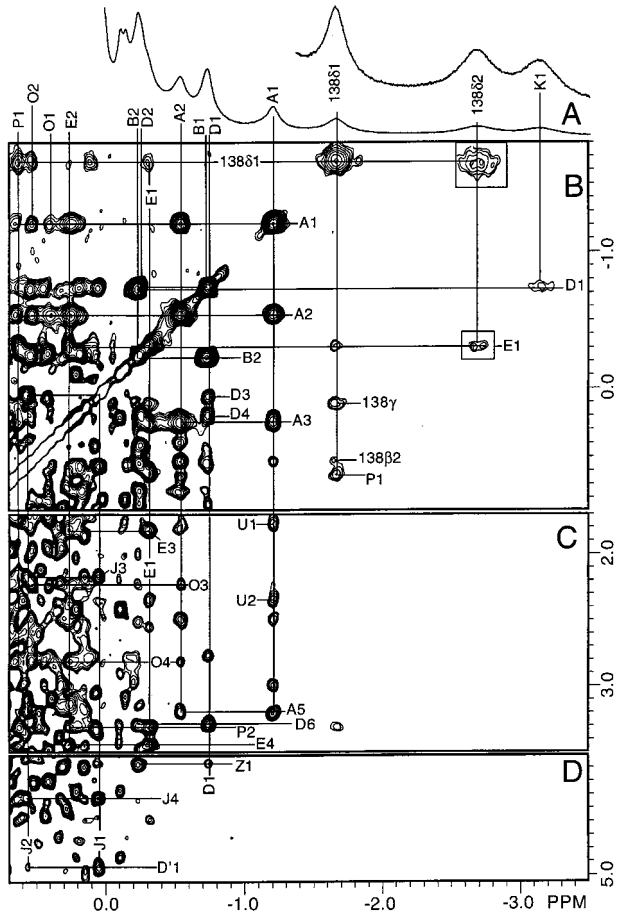

Figure 9. (A) High-field resolved portion of the 600 MHz ^{1}H NMR spectrum of H42A-HRP in ^2H_2O at 30 °C and (B−D) high-field portions of the 600 MHz NOESY spectrum (mixing time = 65 ms) for H42A-HRP in ^2H_2O at 30 °C illustrating the intra- and interresidue contacts for upfield dipolar-shifted aliphatic side chains.

(58) The large variation in α between the two results is not likely significant since the β value is essentially 0.

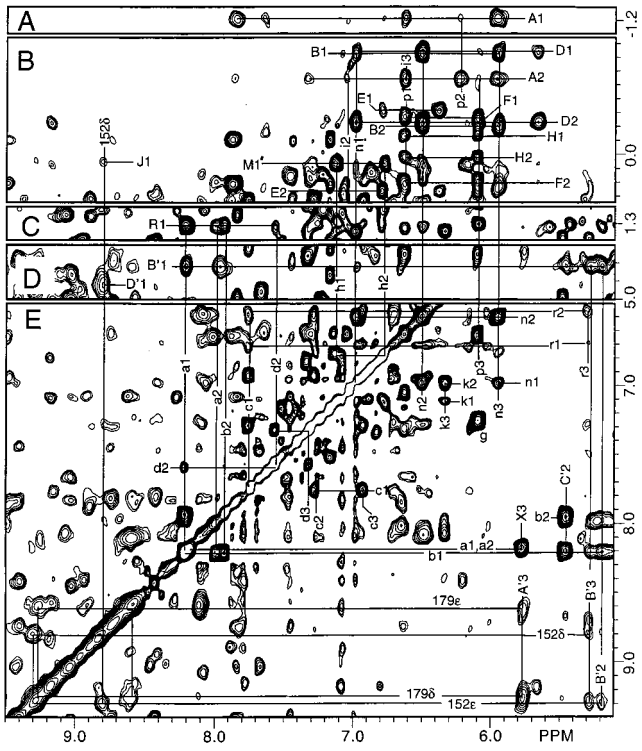

Figure 10. Low-field portion of the 600 MHz NOESY spectrum (mixing time 65 ms) for H42A-HRP in ^2H_2O at 30 °C illustrating (A−E) selected aromatic rings to aliphatic residue contacts and (E) the inter- and intraaromatic ring contacts.

Phe179 ring protons are observed directly upon saturating the heme 3-CH_3, 5-CH_3, and 8-CH_3 peaks (not shown) in a 1D NOE experiment. Essentially the same pattern of NOESY cross-peaks is observed in Figures 9 and 10 for H42A-HRP as in WT HRP, which allows the assignment of the rings of Phe68(*d*), Phe77(*n*), Phe142(*a*), Phe143(*b*), Tyr 234(*p*), Phe266(*k*), Phe273/274(*c*), parts of the spin systems of Leu39(*B*), Ile53(*D*), Leu138, Leu237(*A*), the complete Ala134(*P*), Val46(*E*), Val155(*J*), Gly242(*U*), Val263(O), and $C_\alpha H$(*Z1*) of Asp 43. All exhibit the same pattern of intra- and interresidue NOESY cross-peaks as observed for WT. The two Leu138 $C_\delta H_3$ are again resolved upfield (Figure 9A) and exhibit T_1 values essentially unaltered (33, 50 ms) from those in WT HRP (39, 60 ms). As shown in Figure 9A, however, locating all of the upfield-shifted methyl-containing residues in H42A-HRP that were observed in WT HRP (Figure 6A,B) *leaves unassigned one prominently resolved and strongly relaxed methyl peak K1 at −3.16 ppm in H42A-HRP*. Its relaxation properties ($T_1 \sim 15$ ms), significant upfield δ_{dip}(obs), and the NOESY cross-peak to Ile53 $C_\delta H_3$ (*D1*) (Figure 9B) are consistent only with originating from the mutated Ala42 $C_\beta H_3$, with expected $R_{Fe} = 8.8$ Å. Figure 7 (open circle) shows the good correlation between the observed relaxation rate and predicted R_{Fe} for Ala42 $C_\beta H_3$.

Comparison of the shifts at 30 °C for the assigned residues in WT and H42A-HRP (last two columns in Table 1) reveals that the upfield-shifted residues experience slightly less upfield δ_{DSS}(obs), and the downfield-shifted residues display slightly reduced δ_{DSS}(obs) in H42A-HRP relative to WT HRP. If one assumes an essentially unaltered overall structure between the two proteins, as is confirmed by the highly conserved pattern of dipolar interactions, then the changes in δ_{DSS}(obs) in HRP H42A are due to slightly reduced δ_{dip} in the mutant protein. The reduction of the magnitude of δ_{dip}, without a significant change in the pattern of δ_{dip} among the assigned residues, argues for unchanged orientation of the paramagnetic susceptibility tensor, but a ~10% reduction of D (eq 3) and thus $\Delta\chi_{ax}$ in H42A-HRP relative to WT HRP. Two residues which exhibit larger than 10% changes in δ_{dip}(obs), Leu138 and Ile53, likely have their orientations modified by the adjacent mutation of H42.

Discussion

Scope and Limitation of ^{1}H NMR. The combination of TOCSY and NOESY spectra collected over a wide range of temperatures, analysis of paramagnetic relaxation, the crystal coordinates, and the modeled dipolar shifts allow for a surprisingly effective protocol for assigning a major portion of the "second" and even "third" sphere residues of high-spin ferric HRP. Particularly important assignments are for the aromatic rings (Phes68(*d*), 142(*a*), and 143(*b*)) that influence substrate binding,[11,26] Ala140(*R*) in contact with substrate,[29,54] and Asp247 which serves as a crucial H-bond receptor to the ring of the proximal His170 ring $N_\delta H$.[3] This is by far the most extensive and robust set of assignments of hyperfine shifted resonances for such a large enzyme utilizing solely homonuclear ^{1}H NMR. Moreover, the temperature gradients (d/d(T^{-2})) of the observed shifts serve as remarkably robust indicators of δ_{dip} without requiring any estimates of the diamagnetic shift (see Figures 3 and 8B). The use of Gr(δ_{dip}(obs)), rather than δ_{dip}(obs) from eqs 4 and 9, as an adjunct to assignment protocols becomes more important for high-spin ferric enzymes with distal ligated water, such as cytochrome *c* peroxidase[59,60] for which *D*, and hence $\Delta\chi_{ax}$, are necessarily smaller, and estimates of δ_{DSS}(dia) become even more troublesome in generating δ_{dip} via eqs 4 and 9. The results on H42A-HRP indicate that effective solution structural studies of the influence of point mutations on the heme active site and the substrate binding site can be carried out. The present study sets the stage for quantitative estimates of internuclear distances from NOESY rise curves.[22,61]

Active Site Solution Structure. The pattern of dipolar connections (dependent on the internuclear distance, r_{ij}, as r_{ij}^{-6}), paramagnetic relaxation ($\propto R_{Fe}^{-6}$), and dipolar shifts ($\propto(3\cos^2\theta - 1)R_{Fe}^{-3}$)), in general, is in excellent agreement with the predictions of the crystal structure, although a quantitative comparison must await the direct determination of r_{ij} from NOESY rise curves. One notable discrepancy is observed for Phe68(*d*) in the substrate binding pocket. In the crystal structure of HRP, the Phe68 ring is >5 Å from Phe179, Phe142, and Ala140, but moves much closer to each of these residues upon binding the substrate benzhydroxamic acid, BHA.[30,54] The moderate intensity NOESY cross-peak between Phe68 and both the Phe142(*a*) ring (not shown; see the Supplementary Information) and the methyl of Ala140(*R1*) (Figure 5D), however, indicate that in solution the Phe68 ring orientation is intermediate between that in the crystal of HRP and the BHA:HRP complex.

Dynamic Properties. While the distal side has ready access to water, the proximal side has been shown to be exceptionally stable and impervious to water, as witnessed by the extraordinarily slow exchange rate of not only the peptide NH of axial His170 but its imidazole $N_\delta H$ as well.[15,62] Previous studies on

(59) Finzel, B. C.; Poulos, T. L.; Kraut, J. *J. Biol. Chem.* **1984**, *259*, 13027−13036.
(60) Satterlee, J. D.; Erman, J. E.; La Mar, G. N.; Smith, K. M.; Langry, K. C. *Biochim. Biophys. Acta* **1983**, *743*, 246−255.
(61) Neuhaus, D.; Williamson, M. *The Nuclear Overhauser Effect in Structural and Conformational Analysis*; VCH Publisher: New York, 1989.
(62) La Mar, G. N.; de Ropp, J. S. *Biochem. Biophys. Res. Commun.* **1979**, *90*, 36−41.

HRP-CN located Tyr233 in contact with His170,[29] and showed the former residue to exhibit slow reorientation of its ring, as is the case for the homologous Phe in lignin peroxidase.[63] The present partial characterization of the eight residue proximal aromatic cluster identifies at least two additional slowly reorienting rings: those of Tyr234 and Phe229 (and possibly that of Phe277). Obviously this cluster is densely packed, since at least the rings buried in the cluster center experience significant barriers to rapid rotation right up to the temperature at which HRP denatures above 55 °C. The completely smooth and continuous change in line width and chemical shift, together with conserved and intense interresidue NOESY cross-peak patterns for residues within ~15 Å of the heme, supports a well-defined structure for HRP throughout the temperature range 30−55 °C. Thus the present study finds no support for a structural transition reflected in minor changes in the heme Soret circular dichroism spectra above 40 °C;[64] this small change in the CD could arise from a very local perturbation near the heme that leaves the remaining structure unaltered.

Magnetic Properties. The excellent correlation between Gr[δ_{DSS}(obs)] and $(3\cos^2\theta - 1)R^{-3}$ in Figure 3, and between δ_{dip}(obs) and δ_{dip}(calc) for the optimized magnetic anisotropy in Figure 8B, *confirms that the hyperfine shift of high-spin resting state peroxidases can be quantitatively interpreted in terms of molecular structure and magnetic anisotropy*. The essentially identical $\Delta\chi_{ax}$ determined from the slope in Figure 3 and the fits in Figure 8, using either eqs 4 and 9 or eqs 4 and 10, not only verify the quantitative nature of the determination of the anisotropy, but also establish that, because of the demonstrated T^{-2} dependence of δ_{dip}(obs), *the dipolar shifts arise solely from zero-field splitting, D*. The large data set of dipolar shifts now available confirms that the major magnetic axis is essentially normal to the heme, as observed in both metMbH_2O[41] and ferricytochrome *c*′.[65] The $\Delta\chi_{ax}$ value converts to $D = 9.1$ cm^{-1} via eq 2, assuming a purely high-spin ($\mu_M = 5.92\ \mu_B$) state. If, however, the experimentally measured value of $S = 2.16$ obtained from magnetic susceptibility data[66] ($\mu_M = 5.2\ \mu_B$) is used in eq 2, then $D = 15.3$ cm^{-1}. This value is similar to that for high-spin ferric cytochromes and metmyoglobins[39,40,65] that are five-coordinated (no axial water), and is significantly larger than the $D \sim 8$ cm^{-1} values for six-coordinate ferric hemoproteins.[33,40,41]

Effect of His42 → Ala Mutation. Having established by variable-temperature NOESY the pattern of dipolar contacts among significantly hyperfine shifted residue protons in WT HRP, it is relatively straightforward to assign with reasonable confidence the majority of the active site residues in the mutant protein on the basis of the conserved NOESY contacts, relaxation behavior, and dipolar shift patterns. The conserved pattern of these parameters reflects a largely conserved molecular structure, particularly in regions remote from the His42 mutation. The consistent ~10% decrease in the magnitude of δ_{dip}, except for Leu138 and Ile53, must result from a ~10% decrease in $\Delta\chi_{ax}$, and in turn, *D*. A smaller *D* value necessarily reflects a very slight increase in the effective axial field.[67] It is noted that the *decrease in D in H42A HRP is very slight and its value is still diagnostic of five-*[39,40,65] *rather than six-coordination*.[33,40,41] In globins, mutation of the distal His with a nonpolar residue can, but does not necessarily, alter the state of distal water ligation.[68] Interestingly, resonance Raman spectra of the H42L HRP mutant have been interpreted in terms of a water at the sixth position.[69] The presence of a ligated water with a distal Leu but not Ala is contrary to expectation based on the residue hydrophobicity.[68] The deduced value of *D* for H42A-HRP nevertheless directly supports the absence of a ligated water. The δ_{dip} changes for Ile53 and Leu138 upon mutating His42 are larger than those for any other residue. These results are consistent with the fact that both residues are in contact with His42, and indicate that these two residues have changed their orientation somewhat. More extensive planned assignments, together with NOESY rise curves, may elucidate the orientation of these residues in the mutant.

Conclusions

The present NMR approach demonstrates for the first time that effective and definitive assignment of second sphere resonances are achievable in a moderate sized, high-spin ferric heme enzyme and that the dipolar shifts can be quantitatively interpreted in terms of the molecular and electronic structures of the active site. The assignments of over 40 residues includes the aromatic residues near the substrate-binding pocket, Phe 68, Phe 142, and Phe 179, whose mutation influences substrate binding. Only Phe 68 is shown to have an orientation different from that in the crystal. It is expected that planned NOESY rise-curves will allow quantitative comparison of solution and crystal structures for the heme cavity. The demonstrated methodology, moreover, sets the stage for relatively rapid and effective solution ^{1}H NMR studies of structural changes induced in HRP either by the binding of different substrates[66] or by point mutations in the substrate binding pocket. The characteristic pattern of interproton dipolar contacts and, hence, the heme cavity molecular structure are very largely conserved in the H42A-HRP mutant, including the retention of a five-coordinated heme.

Acknowledgment. The instruments used in this research were funded, in part, by grants from the National Institutes of Health (RR11973, RR04795, RR08206) and the National Science Foundation (90-16484). The research was supported by grants from the National Institutes of Health (GM26226 and GM62830 to G.N.L and GM32488 to P.R.O.M.)

Supporting Information Available: Five figures (55 °C TOCSY spectrum of selected aromatic and downfield $C_\alpha H$ regions of HRP, 55 °C TOCSY spectrum of selected aliphatic regions of HRP, 30 °C NOESY spectrum of selected aromatic and downfield $C_\alpha H$ regions of HRP, 30 °C NOESY spectrum of selected aliphatic regions of HRP, and a plot of δ_{dip}(obs) versus δ_{dip}(calc) for assigned residues from a three-parameter search for α, β, and $\Delta\chi_{ax}$ for HRP at 55 °C), one table (chemical shifts of heme and His170 protons for WT and H42A HRP), and the detailed assignment of the aromatic cluster (PDF). This material is available free of charge via the Internet at http://pubs.acs.org.

JA003687W

(63) Banci, L.; Bertini, I.; Pierattelli, R.; Tien, M.; Vila, A. J. *J. Am. Chem. Soc.* **1995**, *117*, 8659−8667.
(64) Chattopadhyay, K.; Mazumdar, S. *Biochemistry* **2000**, *39*, 263−270.
(65) Déméné, H.; Tsan, P.; Gans, P.; Marion, D. *J. Phys. Chem.* **2000**, *104*, 2559−2569.
(66) Schonbaum, G. R. *J. Biol. Chem.* **1973**, *248*, 502−511.
(67) Brackett, G. C.; Richards, P. L.; Caughey, W. S. *J. Chem. Phys.* **1971**, *54*, 4383−4401.
(68) Springer, B. A.; Sligar, S. G.; Olson, J. S.; Phillips, G. N. *Chem. Rev.* **1994**, *94*, 699−714.
(69) Howes, B. D.; Rodriguez-Lopez, J. N.; Smith, A. T.; Smulevich, G. *Biochemistry* **1997**, *36*, 1532−1543.